

Silicification of Peridotites at the Stalemate Fracture Zone (Northwestern Pacific): Reconstruction of the Conditions of Low-Temperature Weathering and Tectonic Interpretation

S. A. Silantyev^a, A. A. Novoselov^a, E. A. Krasnova^a, M. V. Portnyagin^{a,b}, F. Hauff^b, and R. Werner^b

^a*Vernadsky Institute of Geochemistry and Analytical Chemistry, Russian Academy of Sciences, ul. Kosygina 19, Moscow, 119991 Russia*

e-mail: silantyev@geokhi.ru

^b*Leibniz Institute of Marine Sciences (IFM-GEOMAR), Wischhofstr. 1–3, 24148 Kiel, Germany*

Received May 11, 2011

Abstract—During cruise SO201-1b of the joint Russian–German expedition on the R/V *Sonne* in 2009, mantle peridotites affected by varying secondary alteration were dredged on the eastern slope of the northwestern segment of the Stalemate transverse ridge adjacent to the eponymous fracture zone. The collection discussed in this paper included four samples of silicified serpentinites after dunites and 11 lherzolite samples serpentinized to a varying degree. The abundance of amorphous silica and quartz, very high SiO₂ content (up to 88.7 wt %), and unusually low MgO (up to 1.4 wt %) in the serpentinized dunites strongly distinguish these rocks from the known products of hydrothermal alteration and low-temperature (seafloor) weathering of peridotites in the oceanic crust. In order to determine the conditions and processes resulting in the silicification of peridotites at the Stalemate Fracture Zone, thermodynamic modeling accounting for the kinetics of mineral dissolution implemented in the GEOCHEQ program package was used in this study. The results of modeling allowed us to suppose that the geochemical and mineralogical effects observed in the silicified serpentinized dunites of the Stalemate Fracture Zone are consequences of low-temperature deserpentinization of oceanic materials under subaerial conditions.

DOI: 10.1134/S0869591112010055

INTRODUCTION

Except for the comprehensively studied Emperor seamount chain, information on the structure of the Earth's crust in the northwestern Pacific is currently limited to geophysical data (Erickson and Grim, 1969; Grim and Erickson, 1969) and descriptions of sedimentary cores recovered by deep-sea drilling (Fullam et al., 1973; Rea and Dixon, 1973; *Shipboard Scientific...*, 1993). The nature of the oceanic basement in this oceanic region is very poorly known and remains a terra incognita in the existing concepts on the geologic history of the Pacific. The most detailed interpretation of the geodynamic evolution of the lithosphere in the northwestern Pacific on the basis of geophysical and paleomagnetic data was proposed by Lonsdale (1988). According to this interpretation, a small fragment of the ancient and previously considered hypothetical Kula plate was preserved in the northwestern sector of the Pacific Ocean south of the Aleutian Trench. This fragment is bordered in the south by the extended transverse Stalemate Ridge adjacent to a supposed paleotransform fault of the Kula–Pacific spreading center. This ridge extends over more than 500 km from the southeast to the northwest and was supposedly formed by the tectonic uplift of an oceanic lithospheric block of Cretaceous (?) age along the

transform fault (Lonsdale, 1988). However, no data were available on the rocks of the Stalemate Ridge.

The Stalemate Fracture Zone was a subject of study of cruise SO201-1b of 2009 of the German R/V *Sonne* within the German–Russian project KALMAR. The results of multibeam bathymetry performed during the cruise (Fig. 1) supported the conclusions of previous studies (Lonsdale, 1988) and allowed reliable interpretation of this rise as a transverse ridge. Morphologically, the Stalemate Ridge is similar to transverse ridges parallel to the adjacent transform faults in modern oceanic basins formed owing to the tectonic uplift of the oceanic lithosphere along the fracture zones (Bonatti, 1978; Kastens et al., 1998; Bonatti et al., 2005). A remarkable achievement of this cruise was successful dredging at four stations along the Stalemate Ridge (Fig. 1), which recovered rocks representing the complete section of the oceanic lithosphere formed in the Kula–Pacific spreading center (*FS Sonne...*, 2009).

The rocks considered in this paper were obtained at dredge station DR37 on the eastern slope of the northwestern segment of the Stalemate Ridge in a region with ocean depths of 4600–3000 m (Fig. 1). Dredging was carried out at depths of 4360–3955 m and recovered fragments of strongly altered ultrabasic rocks

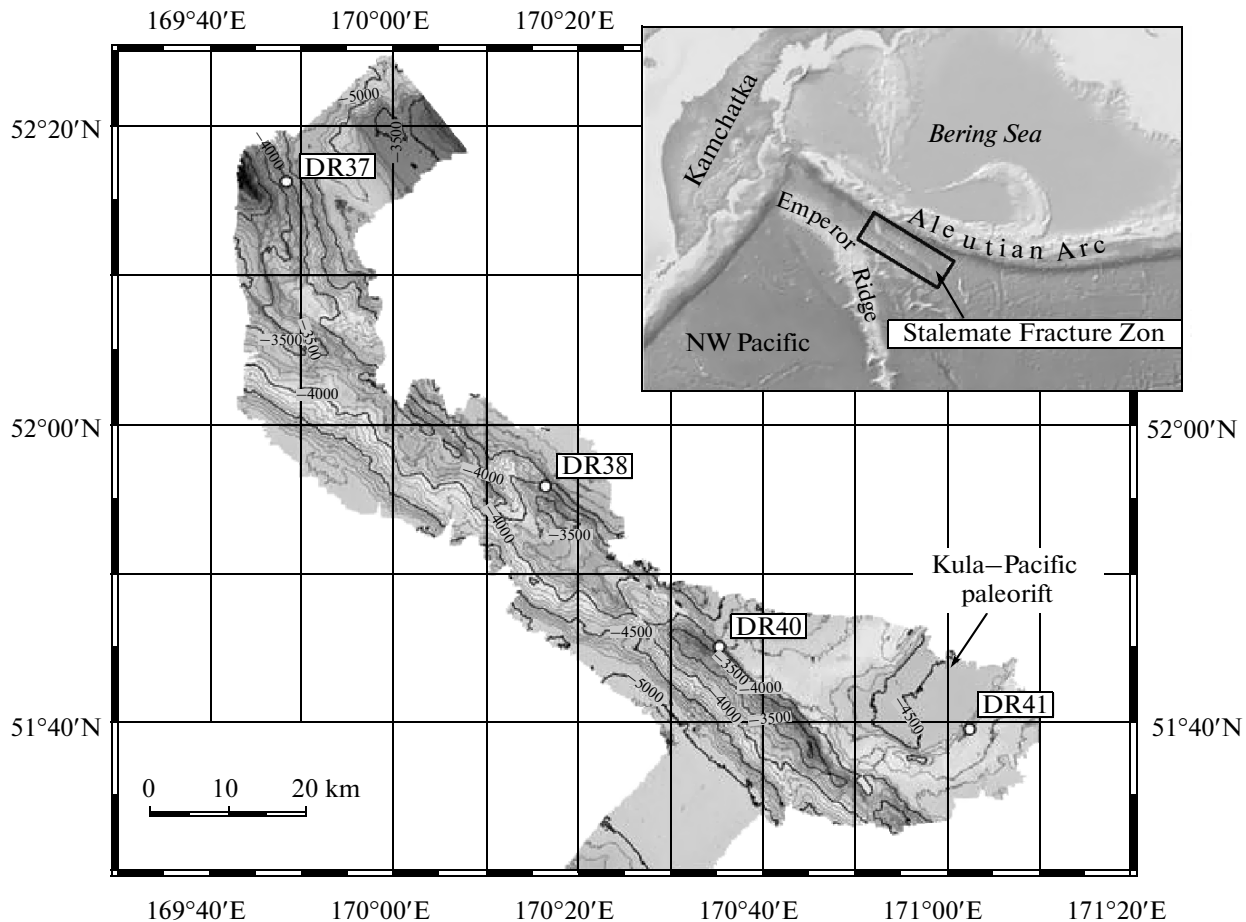


Fig. 1. Topographic map of the ocean floor and the location of dredge stations of the R/V *Sonne* at the region of the Stalemate Transform Zone. The detailed map is based on the data of multibeam bathymetry obtained during cruise SO201-1b of the R/V *Sonne* within the German–Russian project KALMAR and was constructed onboard using the GMT program package of Wessel and Smith (1995). The overview map was constructed using the GeoMapApplication program (<http://www.geomapp.org>; Ryan et al., 2009).

including, according to the onboard description, serpentinized dunites, harzburgites, and lherzolites (*FS Sonne*..., 2009). The goal of this study was the reconstruction of the conditions of low-temperature alterations of the peridotites of the Stalemate Ridge and identification of related processes.

METHODS

The peridotite samples selected for investigations were crushed at IFM–GEOMAR (Kiel, Germany). For chemical analysis, a 1–5 mm fraction was rinsed with deionized water and ground in a jasper planetary ball mill to 200 mesh at the same research center. The <1 mm fraction was used for hand-picking mineral separates, which were mounted for electron microprobe analysis.

In order to determine major element contents, powdered rocks were fused with $\text{Li}_2\text{B}_4\text{O}_7/\text{LiBO}_2$ and analyzed by X-ray fluorescence (XRF) at ACME laboratories (Vancouver, Canada). The analytical back-

ground was smaller than 0.01 wt % for all elements. The measurement of standard samples indicated an analytical accuracy of 0.02% relative and a precision of 0.01% relative.

For trace element analysis, the powdered rocks were mixed with epoxy resin (Buehler EpoThin) and mounted in separate cells of a Plexiglas disk. The amount of powder mixed with epoxy resin varied from sample to sample and was usually 20–40%. After solidification, the mounts were polished using corundum paper with a particle size of up to 12 μm . Powdered rock standards (AGV-2, BCR-2, BHVO-2, BIR-1, and W-2) were prepared in the same fashion. Analyses were performed at the Institute of Earth Sciences of Christian–Albrecht University (Kiel, Germany) by laser ablation–inductively coupled plasma mass spectrometry. The Geolas Pro (Coherent) ablation system included a COMPexPro™ excimer laser coupled with an Olympus microscope and an Agilent 7500c quadrupole inductively coupled plasma mass spectrometer. Each peridotite and standard sample

were analyzed twice. The NIST612 and BCR-2G glasses (Jochum et al., 2009) were used for primary calibration. All the samples and standards were analyzed using the same procedure, which included background measurement over 20 s and sample analysis over 250 s along a 1-mm-long line. The laser beam diameter was 80 μm at an laser energy density of 10 J/cm² and a repetition rate of 10 Hz. The contents of elements were calculated using calibration lines based on the measurement of standards in the coordinates of element to SiO₂ ratio versus the ratio of the measured intensities of the appropriate element isotope and ³⁰Si. The ²³²Th¹⁶O⁺/²³²Th⁺ ratio was lower than 0.5% during analyses, which indicates a high degree of the dissociation of complex ions in the plasma and their negligible influence on the analytical results. The analyses of standard samples are given in Table 2.

The compositions of major minerals were determined at the Vernadsky Institute of Geochemistry and Analytical Chemistry, Russian Academy of Sciences (supervised by N.N. Kononkova) using an SX 100 Cameca electron microprobe with four vertical spectrometers at an accelerating voltage of 15 kV and a beam current of 30 nA. The compositions of tremolite, titanite, and epidote in samples DR37-8 and DR37-15 and element distribution maps in the silicified serpentinite samples were obtained at IFM–GEOMAR using a JEOL JXA 8200 electron microprobe.

PETROGRAPHY AND GEOCHEMISTRY OF PERIDOTITES FROM THE STALEMATE RIDGE

Petrographic and Mineralogical Characteristics

The peridotite collection included four samples of strongly altered dunitic rocks and 11 samples of altered lherzolites. According to Krasnova et al. (2011), the spinel lherzolites were produced by the 10–12% near fractional melting of the depleted mantle, and the dunites could result from lherzolite–melt interaction. The strongly altered dunites are light red rocks with rare (<3%) macroscopically visible spinel relicts (*FS Sonne...*, 2009). The petrographic examination of these rocks revealed a reticulate texture typical of altered dunites (Fig. 2). However, the main mineral of the altered dunites is quartz rather than serpentine. There are very subordinate amounts of chlorite, serpentine, and iron hydroxides and rare relicts of primary reddish brown spinel and bottle-green clinopyroxene (Fig. 2). The almost complete silicification clearly distinguishes the serpentized dunites from the known products of hydrothermal alteration and low-temperature (seafloor) weathering of peridotites in the oceanic crust (Silantyev et al., 2009). Up to now, such a phenomenon has never been described in the literature on the mineralogy and geochemistry of peridotites from the basement of modern ocean basins.

Most of the peridotite samples from our collection are serpentinites after spinel lherzolites. These rocks show rather significant variations in textural characteristics, and there are varieties with reticulate and bastite textures. It is evident that the textural diversity of the serpentinites is controlled mainly by the mineralogy of the initial rocks. Some peridotite samples of this group show distinct indications of syntectonic recrystallization (sample DR37-15). They have a banded structure, and bending of individual layers composed of tremolite and minor talc is clearly observed in thin sections. In contrast to the silicified dunites, the serpentized lherzolites show much better preservation of primary minerals, among which orthopyroxene, clinopyroxene, and abundant spinel were identified. These rocks bear diverse secondary mineral assemblages corresponding to the wide temperature range of their formation.

The compositions of secondary minerals from the serpentinites of the Stalemate Ridge are given in Table 1. Chlorite from the altered dunitic rocks is clinochlore with high chromium content. This peculiarity of chlorite composition is probably mainly due to its formation by the recrystallization of primary spinel. High chromium contents in chlorite from the serpentinites of the Mid-Atlantic Ridge (MAR) have been reported in many publication on oceanic core complexes (e.g., Bazylev, 1997; Silantyev et al., 2011). Serpentine from the serpentized lherzolites of the Stalemate Fracture Zone is chemically similar to serpentized peridotites from the oceanic core complexes of the MAR (e.g., Silantyev et al., 2011) and shows variable Al₂O₃ (0.34–2.3 wt % and 0.95–3.3 wt % in two samples) and a positive correlation between Fe and Cl contents. The finding of clinozoisite in a sample of tectonically affected banded serpentinite (DR37-16) may indicate the presence of plagioclase in this rock. Titanite was found in sample DR37-8, although this mineral is not typical of oceanic serpentinites. However, this phase is often observed in vein gabbroids associating with abyssal peridotites, where it replaces ilmenite or titanomagnetite (e.g., Silantyev et al., 2011). Perhaps, the serpentized lherzolites of the Stalemate Fracture Zone contain thin veinlets of gabbroid material, the presence of which could be disguised by serpentization. Among the secondary minerals of the serpentized lherzolites, a mixed-layer phase replacing orthopyroxene was also detected. This phase is a talc–chlorite mixture (Table 1). A similar phase was previously reported by Bazylev (1997) from the metaperidotites of the Hayes Fracture Zone. The temperature of formation of the tremolite + chlorite + talc assemblage in the peridotites was estimated as 450–500°C (Bazylev, 1997). Thus, as was noted above, the serpentized lherzolites of the Stalemate Fracture Zone show evidence for relatively high-temperature intracrustal oceanic metamorphism. It should be pointed out that some samples of serpentized lherzolites contain quartz (or amorphous silica), the content of which is much lower than that in the

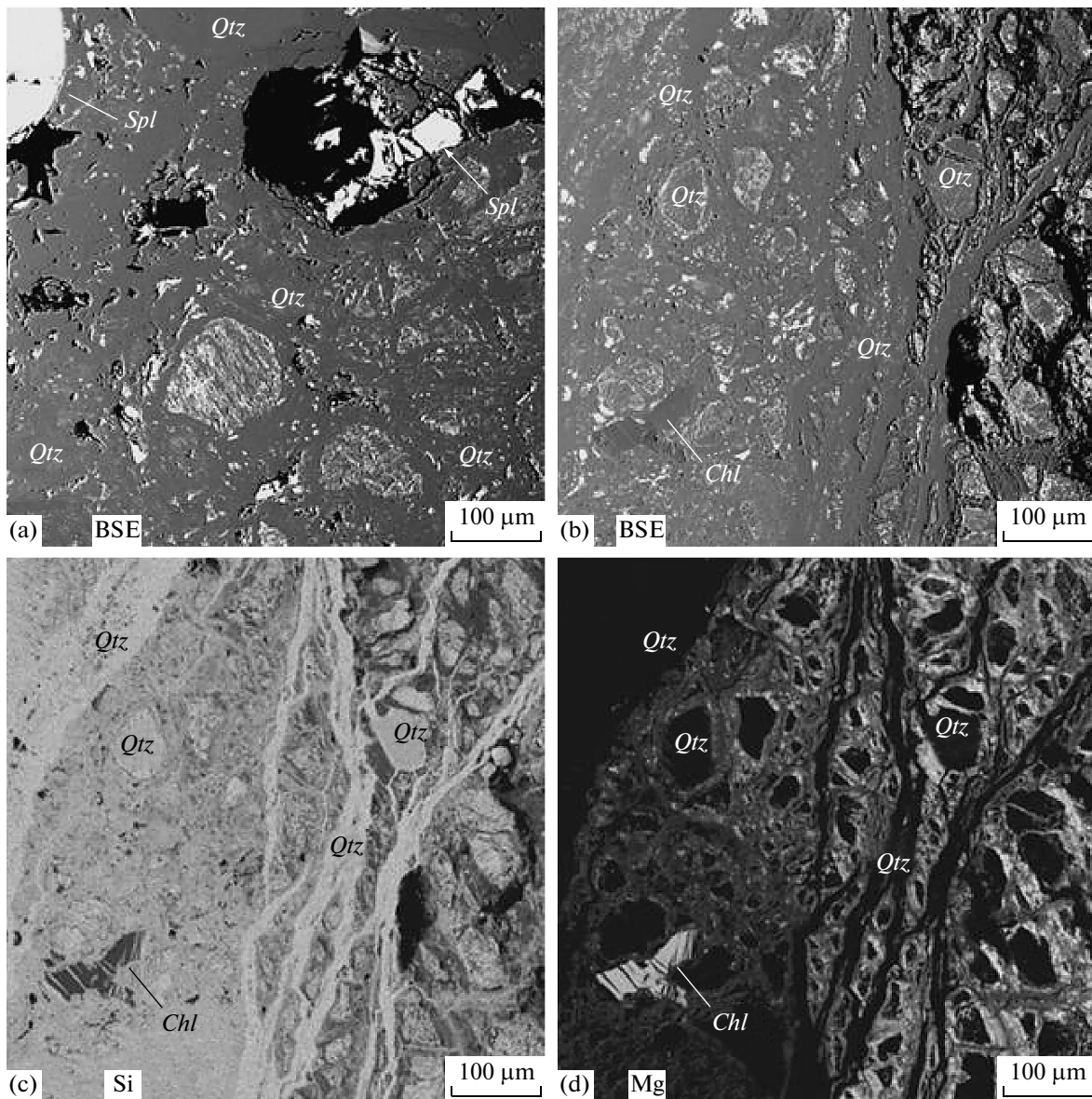


Fig. 2. Structures of silicified dunites from the Stalemate Fracture Zone. (a) Back-scattered electron image of a fragment of sample DR37-2. The bulk SiO_2 content in this rock is 87 wt %. Former olivine cores are replaced by a microcrystalline aggregate of quartz with admixtures of iron oxides, and the matrix is pure quartz. Relicts of chrome spinel are present. (b)–(d) Fragment of sample DR37-4 from a transition zone between the brecciated (right) and massive (left) zones. (b) Back-scattered electron image; (c) distribution of Si contents; (d) distribution of Mg contents. Lighter areas in Figs. 2c and 2d correspond to higher contents, and darker areas correspond to lower contents. The bulk SiO_2 content in the rock is 71 wt %. Former olivine cores and cross-cutting veins are composed of microcrystalline and amorphous quartz. A relict chlorite grain occurs in the lower left of the fragment. The matrix is composed of a quartz aggregate with admixtures of magnesium and iron oxides, the proportions of which are somewhat different in the massive and brecciated parts of the rocks. The massive part is relatively richer in SiO_2 . All images were obtained at IFM–GEOMAR using a JEOL 8200 electron microprobe at an accelerating voltage of 20 kV and a beam current of 30 nA. Element mapping was carried out with a step of 1 μm and a counting time of 50 ms at each spot.

altered dunites. The latter are referred to below as silicified serpentinites after dunites on the basis of the aforementioned feature and geochemical characteristics.

Geochemistry of the Peridotites of the Stalemate Ridge

The contents of major and selected trace elements in the silicified serpentinites after dunites and serpen-

tinized lherzolites of the Stalemate Fracture Zone are given in Table 2.

Figure 3a illustrates peculiar features of the silicified dunites: very high SiO_2 (up to 88.70 wt % in sample DR37-2) and unusually low MgO contents (1.39 wt % in the same sample). Also shown in Fig. 3a are the compositional fields of MAR abyssal peridotites (collection of more than 250 samples from the

Table 1. Compositions of major secondary minerals in the peridotites of the Stalemate Ridge, wt %

Component	DR37-1	DR37-1	DR37-5	DR37-5	DR37-5	DR37-5	DR37-8	DR37-9	DR37-9	DR37-9	DR37-14	DR37-14
	1	1	2	2	2	2	2	2	2	2	2	2
	<i>Chl</i>	<i>Chl</i>	<i>Ta+Chl</i>	<i>Srp</i>	<i>Srp</i>	<i>Tr</i>	<i>Spn</i>	<i>Srp</i>	<i>Tr</i>	<i>Srp</i>	<i>Tr</i>	<i>Tr</i>
SiO ₂	31.86	32.62	53.36	49.42	38.4	56.65	30.89	40.58	51.11	39.07	55.45	55.05
TiO ₂	0.06	0.03	0.01	0.02	0.01	0.05	35.14	0.01	0.07	0.01	0.05	0.08
Al ₂ O ₃	15.69	15.42	2.02	3.28	0.95	2.69	0.29	0.34	4.21	2.3	3.84	3.96
FeO	2.99	2.98	2.64	4.58	10.26	1.82	0.69	6.51	3.05	6.85	4.25	3.99
MnO	0.02	0	0	0.02	0.11	0.07	0.02	0.03	0.12	0.16	0.08	0.12
MgO	33.58	34.22	28.16	31.05	30.72	23.03	0.02	35.26	20.29	37.43	25.87	25.49
CaO	0	0.01	0.12	0.15	0.18	13.26	29.14	0.08	12.25	0.33	10.28	10.94
Na ₂ O	0.02	0.01	0.29	0.24	0.08	0.3	0	0.18	0.59	0.04	0.11	0.14
K ₂ O	0.01	0.01	0.04	0.06	0.06	0.02	0.01	0.06	0.03	0	0.01	0
Cr ₂ O ₃	2.1	2.32	0.7	0.8	0.08	0.41	0	0.07	2.1	0.77	0.95	0.89
NiO	0.02	0.02	0.02	nd	0.01	0.18	0.07	nd	0.04	nd	0.15	0.06
Cl	nd	nd	0.02	0.04	0.48	nd	nd	0.17	0.04	0.24	nd	nd
Total	86.36	87.64	87.39	89.66	81.33	98.49	96.27	83.3	93.91	87.19	101.05	100.72
Component	DR37-15	DR37-15	DR37-15	DR37-15	DR37-15	DR37-15	DR37-15	DR37-15	DR37-15	DR37-15	DR37-15	DR37-15
	2	2	2	2	2	2	2	2	2	2	2	2
	<i>Tr</i>	<i>Tr</i>	<i>Tr</i>	<i>Tr</i>	<i>Tr</i>	<i>Tr</i>	<i>Tr</i>	<i>Tr</i>	<i>Tr</i>	<i>Tr</i>	<i>Tr</i>	<i>Zo</i>
SiO ₂	55.32	55.12	53	55.54	58.23	57.5	52.3	58.52	52.23	57.96	38.44	
TiO ₂	0.04	0.05	0.1	0.02	0.04	0.03	0.54	0.06	0.38	0.11	0.11	
Al ₂ O ₃	3.23	3.9	5.85	3.13	0.79	0.68	6.06	0.74	5.39	1.07	28.32	
FeO	1.91	2.01	2.3	1.79	2.72	2.66	2.43	2.44	2.38	1.54	8.54	
MnO	0	0	0.05	0.06	0.08	0.12	0.06	0.09	0.03	0	0.01	
MgO	21.9	21.81	21.09	22.4	22.87	22.86	21.02	23.07	21.63	23.59	2.15	
CaO	13.54	13.44	13.33	13.27	13	12.88	13.45	13	13.22	13.23	21.64	
Na ₂ O	0.54	0.67	1.09	0.64	0.21	0.18	1.1	0.17	1.1	0.23	0.02	
K ₂ O	0.02	0.02	0.04	0.01	0.01	0.01	0.05	0.01	0.01	0.01	0.01	
Cr ₂ O ₃	0.87	0.95	1	0.43	0	0.06	0.69	0.02	0.77	0.28	0.04	
NiO	0.14	0.2	0.19	0.13	0.08	0.15	0.16	0.15	0.09	0.11	0.04	
Cl	nd	nd	nd	nd	nd	nd	nd	nd	nd	nd	nd	
Cymma	97.5	98.16	98.04	97.43	98.03	97.13	97.86	98.27	97.52	98.14	99.31	

Note: 1, serpentinites after dunite and 2, serpentinitized lherzolites. Mineral symbols: *Chl*, chlorite; *Ta + Chl*, mixed-layer phase; *Srp*, serpentine; *Tr*, tremolite; *Spn*, titanite; and *Zo*, zoisite. nd indicates not determined.

Table 2. Contents of major and selected trace elements in the peridotites of the Stalemate Ridge

Com- ponent	DR37-1	DR37-2	DR37-3	DR37-4	DR37-5	DR37-6	DR37-8	DR37-9	DR37-10	DR37-11	DR37-12	DR37-13	DR37-14	DR37-15	Stan- dard	Stan- dard	Stan- dard
	1	1	1	1	2	2	2	2	2	2	2	2	2	2	3	3	4
SiO ₂	83.7	88.7	85.6	71.1	39.9	40.8	40.2	41.3	39.8	41.7	39.9	40.7	39.3	41.6	50	49.9	49.0
TiO ₂	0.07	0.04	0.07	0.05	0.03	0.04	0.1	0.05	0.04	0.06	0.05	0.04	<0.01	0.18	0.27	0.27	0.28
Al ₂ O ₃	0.2	0.19	0.13	0.48	1.91	1.78	3.26	2.36	2.09	3.25	1.83	2.02	2.07	3.26	20.67	20.68	20.69
Fe ₂ O ₃	6.54	6.53	5.39	9.44	11.94	12.4	9.67	11.3	9.9	11.13	11.33	10.6	10.48	11.44	6.3	6.28	6.21
MnO	0.09	0.06	0.05	0.23	0.15	0.2	0.43	0.75	0.23	0.13	0.1	0.1	0.21	0.23	0.11	0.11	0.108
MgO	4.9	1.39	4.56	10.24	28.92	28.4	29.54	27.64	31.52	28.31	30.56	30.44	31.32	27.15	0.52	0.52	0.54
CaO	0.03	0.04	0.03	0.06	1.62	0.96	1.05	2.21	1.51	2.1	1.69	1.94	1.15	2.78	8.07	8.07	8.05
Na ₂ O	0.09	0.07	0.09	0.13	0.3	0.34	0.49	0.42	0.3	0.36	0.26	0.28	0.33	0.38	7.17	7.14	7.1
K ₂ O	0.07	0.06	0.08	0.07	0.12	0.14	0.17	0.15	0.1	0.16	0.1	0.11	0.11	0.14	1.63	1.61	1.66
P ₂ O ₅	0.03	0.06	0.02	0.05	0.04	0.03	0.03	0.04	0.03	0.03	0.03	0.03	0.03	0.05	0.13	0.12	0.131
L.O.I.	3.74	2.26	3.45	7.05	14.62	14.98	15.39	13.79	14.59	12.86	14.3	13.99	15.24	12.55			
Total	99.47	99.36	99.44	98.94	99.56	100.04	100.35	100.01	100.11	100.12	100.18	100.26	100.27	99.73			
Sc	3.76	3.25	3.20	4.31	10.41	8.89	9.50	13.20	9.29	12.04	11.44	11.82	10.78	14.18	34.3	33.1	33
Cr	331	2830	386	1011	1362	1635	2158	1802	1033	1639	1056	1288	1577	2271	<20	<20	18
Co	97.1	79.6	56.8	124.1	93.8	122	200.2	192.3	95.3	138.6	80.8	66.7	87.6	110	38.2	38.2	37.0
Ni	802.9	546.9	602.9	920.8	1726	1677.5	1440.3	1695.5	1456.5	1283.7	1642.9	1771.1	1460.7	1425.8	9.7	10.2	18.0
Sr	8.66	8.36	7.10	12.78	17.08	16.67	26.81	24.72	14.28	15.36	13.99	13.54	13.98	19.04	350	364	340

Note: 1, serpentinites after dunite; 2, serpentinitized lherzolites; 3, STD SY-4(D) for major elements (SiO₂-P₂O₅) and BCR-2 for Sc, Cr, Co, Ni, and Sr; and 4, expected values for the standards. Oxides are in wt %, and elements are in ppm.

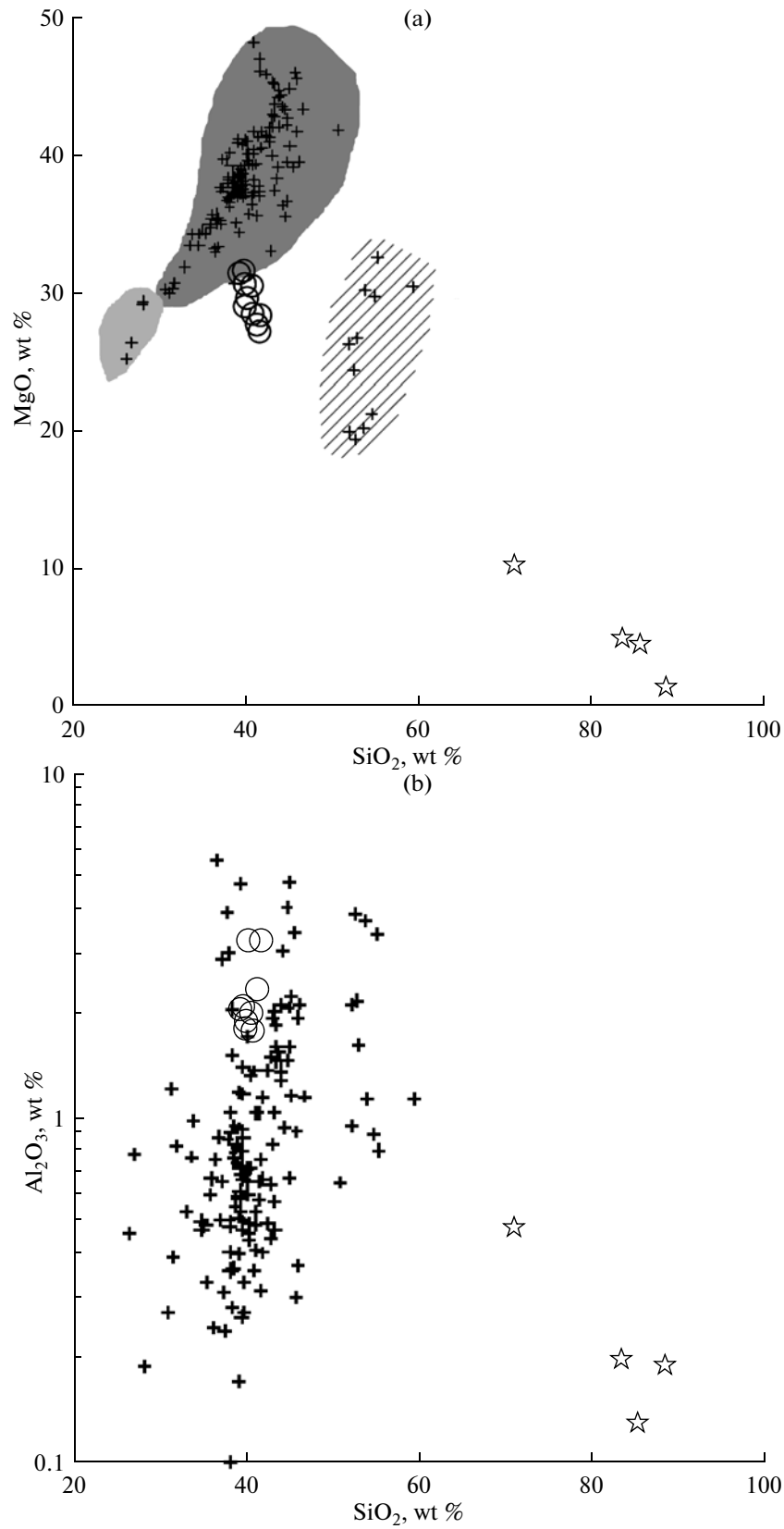


Fig. 3. Covariations of the contents of (a) SiO₂ and MgO, (b) SiO₂ and Al₂O₃, (c) SiO₂ and CaO, (d) SiO₂ and FeO*, (e) SiO₂ and Na₂O, (f) SiO₂ and Ni, and (g) SiO₂ and Sc in the peridotites of the Stalemate Ridge. Asterisks are silicified dunitic rocks, circles are serpentinized lherzolites, and crosses are abyssal peridotites from MAR. The dark gray field shows the compositions of serpentinites, the light gray field is carbonized serpentinites, and oblique hatching shows the compositions of steatitized peridotites.

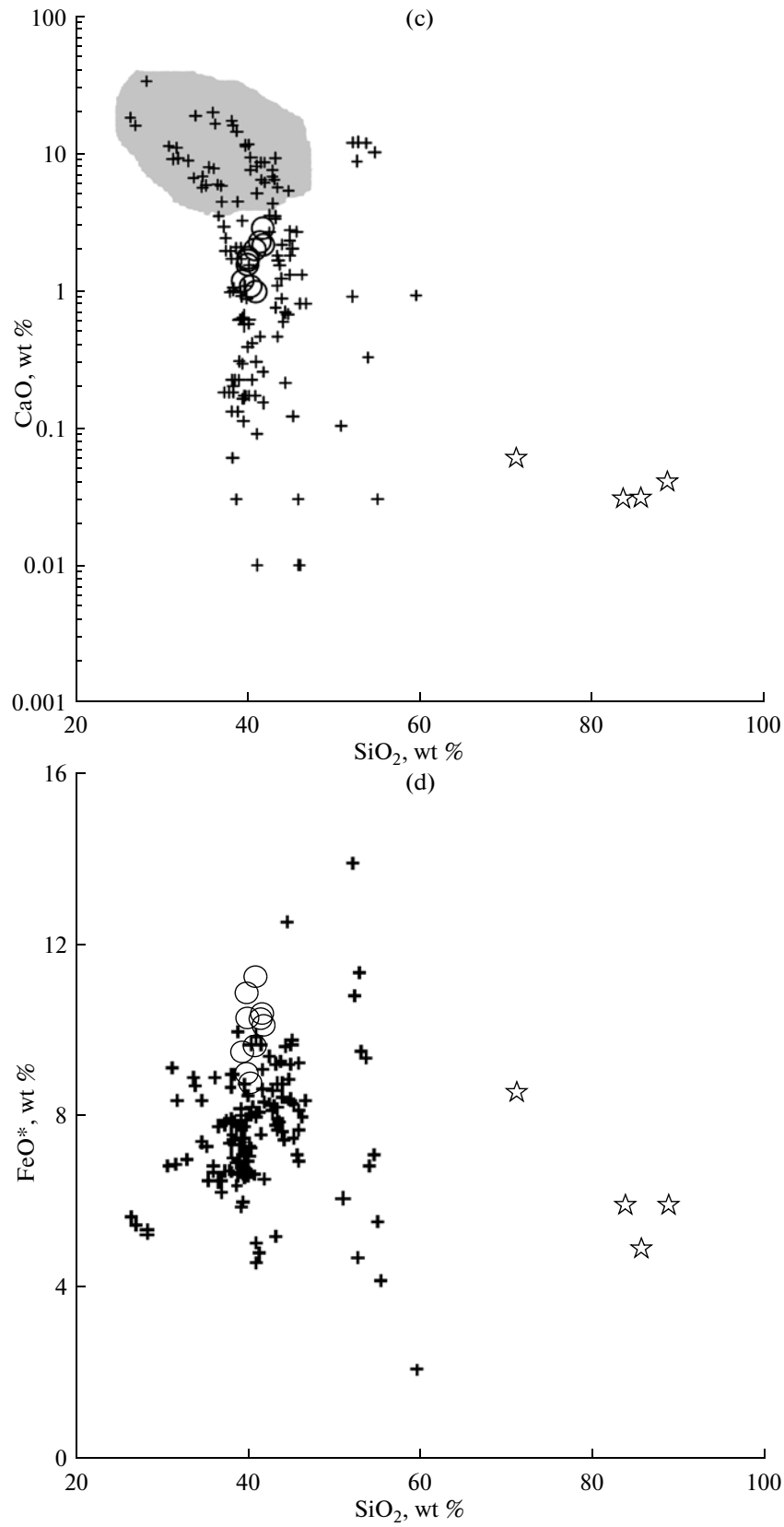


Fig. 3. (Contd.)

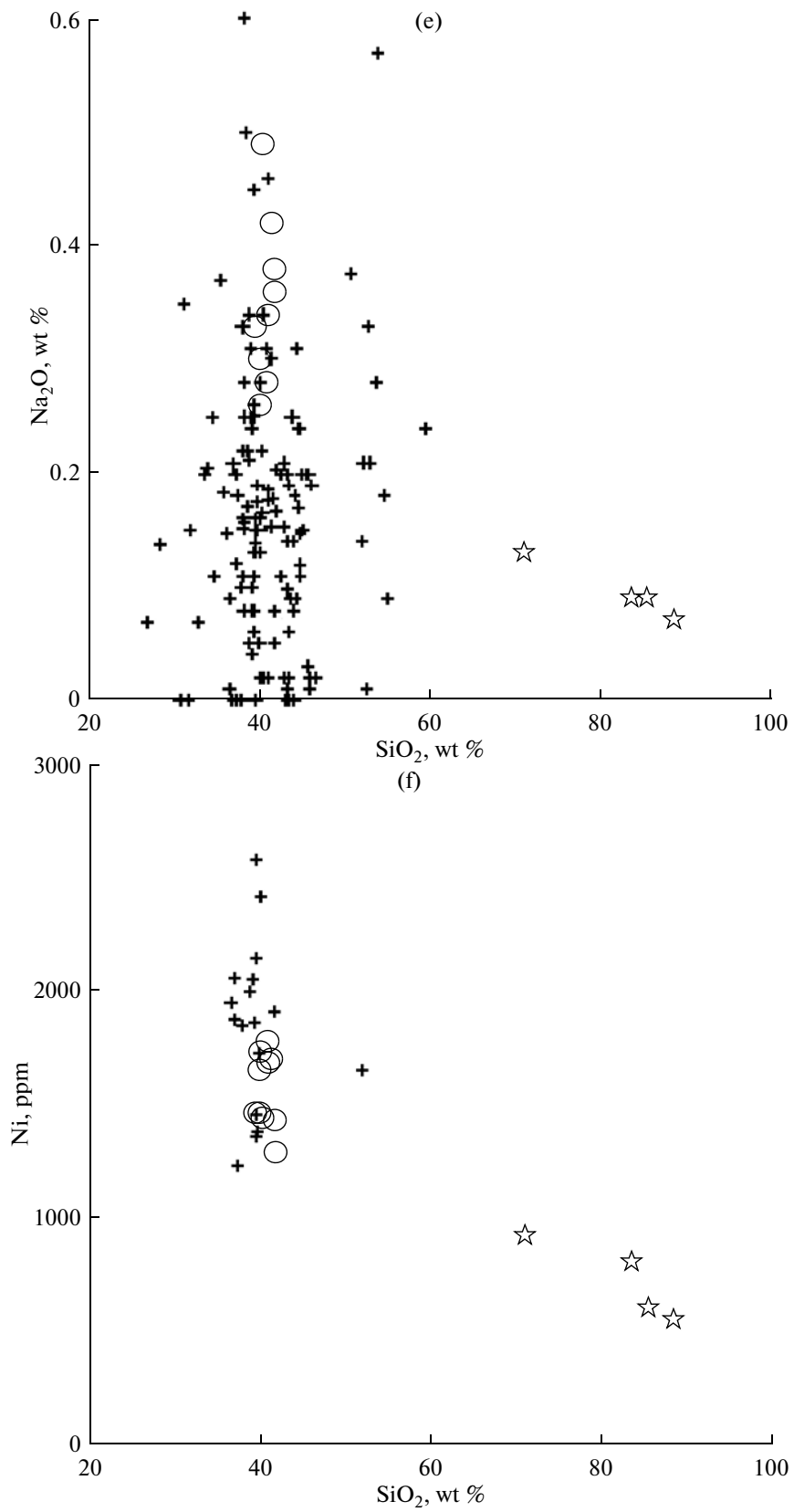


Fig. 3. (Contd.)

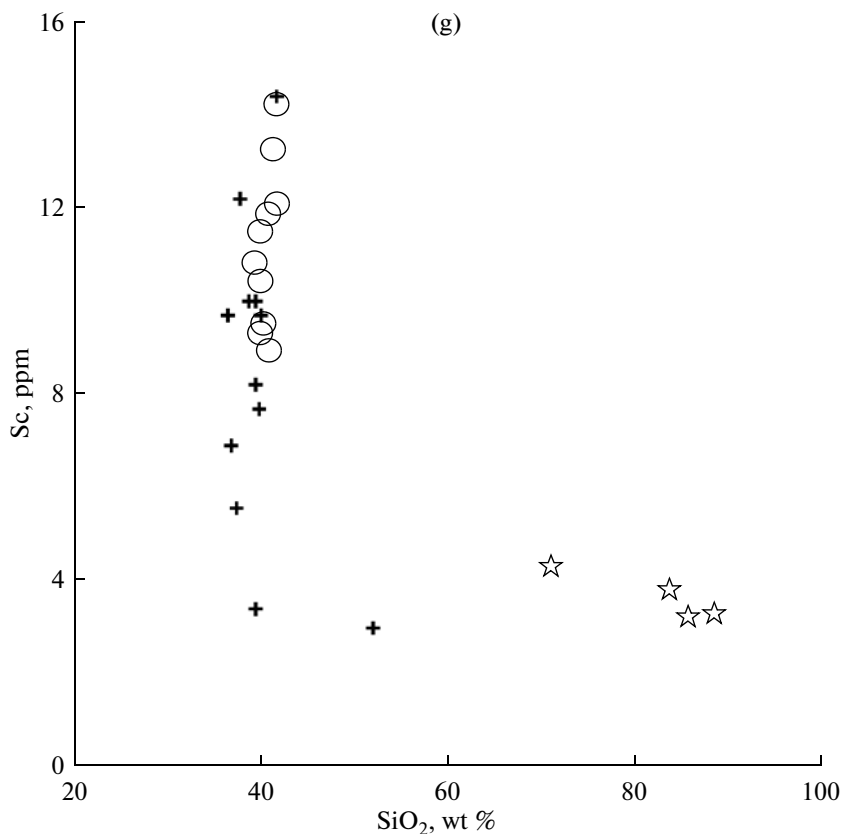


Fig. 3. (Contd.)

crest zone of the ridge between 12°N and 51°N), separately for serpentinites, carbonated serpentinites, and peridotites that underwent steatitization (replacement by talc). The distribution of the compositions of the silicified dunites of the Stalemate Ridge in the SiO₂—MgO diagram emphasizes the sharp difference of these rocks from the products of hydrothermal alteration of oceanic ultrabasic rocks. The negative correlations of SiO₂ with Al₂O₃, CaO, FeO, Na₂O, Ni, and Sc in the altered dunites indicate that the silicification was accompanied by the replacement of ferromagnesian silicates in the protolith of these rocks by quartz (Figs. 3b–3g). In contrast, the serpentinitized lherzolites are compositionally similar to abyssal peridotites. Nonetheless, these rocks also show geochemical evidence for the initial stage of silicification, for instance, a negative correlation between SiO₂ and MgO and some enrichment of the serpentinitized lherzolites in SiO₂ compared with the MAR peridotites.

The extrapolation of the compositions of the silicified dunites into the supposed region of the initial rocks provides an approximate estimate for the composition of their protolith: ~1 wt % Al₂O₃, ~6 ppm Sc, and ~1800 ppm Ni. The lower contents of Sc and Al₂O₃ and higher Ni contents in the protolith of the altered dunites compared with the serpentinitized lherzolites suggest that the protolith of the silicified ser-

pentinites was depleted in pyroxenes and enriched in olivine compared with the lherzolites. Thus, the geochemical data support the primary dunitic nature of the protolith of the silicified serpentinites. It should be pointed out that the silicification of the peridotites was accompanied by their deserpentinitization and, consequently, was a later process. This is indicated by the strong negative correlation between SiO₂ content and loss on ignition for the silicified dunites (Fig. 4a).

The obtained data indicate that the serpentinitized lherzolites dredged at the Stalemate Fracture Zone were undoubtedly metamorphosed within a wide temperature range under oceanic crustal conditions. On the other hand, the silicified serpentinites have no mineralogical and geochemical analogues among abyssal peridotites. Hence, the deserpentinitization and silicification of these rocks reflect a more complex evolution of oceanic materials compared with that recorded in the composition of all known abyssal peridotites.

Thus, taking into account the modern setting of the silicified dunites on the deep-sea slope of a submarine ridge in the zone of an oceanic transform fault, the reconstruction of the conditions of low-temperature alterations resulting in the silicification of peridotites becomes fundamentally important for the understanding of the general character of the evolution of

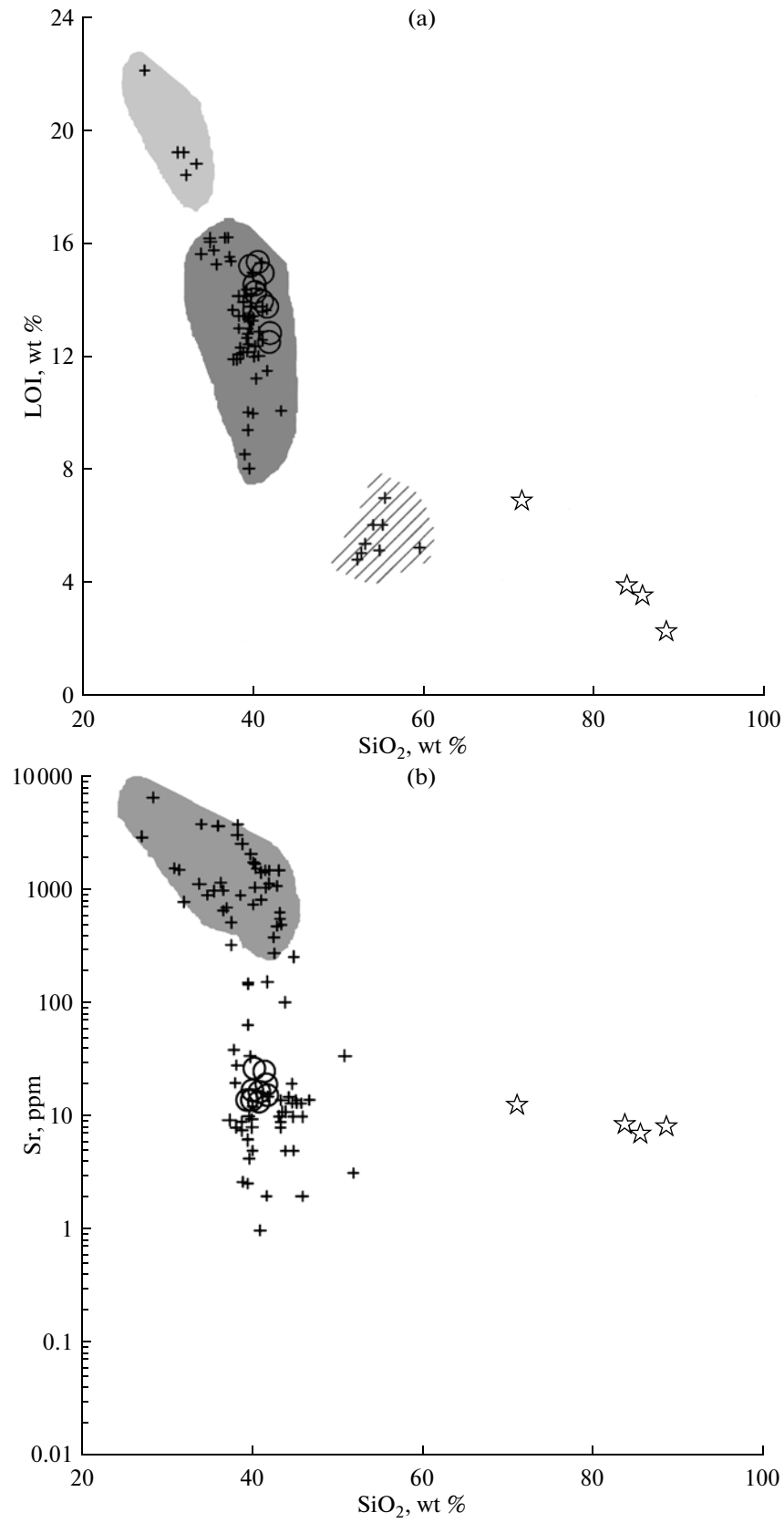


Fig. 4. Covariations of (a) SiO₂ and LOI and (b) SiO₂ and Sr in the peridotites of the Stalemate Fracture Zone. Symbols are the same as in Fig. 3.

the northwestern segment of the Kula–Pacific paleofracture zone.

ESTIMATION OF CONDITIONS AND PROCESSES OF PERIDOTITE SILICIFICATION AT THE STALEMATE FRACTURE ZONE

Processes of Peridotite Alteration in the Oceanic Crust: An Overview of Available Data

The tremendous amount of data accumulated up to now indicates that almost all available samples of abyssal peridotites were affected to a varying degree by medium-temperature hydrothermal alteration and low-temperature submarine weathering (or halmyrolysis). Silant'ev et al. (2009) used numerical methods for a wide temperature range and distinguished in the section of the oceanic crust five characteristic mineral facies of hydrothermally altered peridotites from slow-spreading MOR: (1) aragonite–goethite–saponite (20–65°C); (2) chrysotile–hematite–pyrite (65–130°C); (3) chrysotile–magnetite–pyrrhotite (130–260°C); (4) antigorite–tremolite–magnetite–pyrrhotite (260–410°C); and (5) talc–tremolite–olivine–magnetite–pyrrhotite (410–480°C). The secondary minerals of the lherzolites of the Stalemate Fracture Zone are tremolite, talc, titanite, clinozoisite (only in sheared serpentine sample DR37-15), chlorite, and serpentine. Thus, the aforementioned secondary phases occurring in the serpentinized lherzolites correspond to the whole spectrum of the mineral types of hydrothermally altered peridotites in the oceanic crust and were formed under the conditions of the retrograde branch of oceanic metamorphism. The medium-temperature stage of the metamorphism of the Stalemate Ridge peridotites occurred in the lower levels of the oceanic crust and predated the serpentinization and low-temperature alteration of the rocks.

The main exogenous agent controlling the geochemical trends of the intracrustal transformation of the mantle peridotites of MOR is seawater and its derivatives interacting with the whole section of the oceanic crust. Among the most reliable indicators for the degree of alteration of ultramafic rocks of the oceanic basement are the $^{87}\text{Sr}/^{86}\text{Sr}$ ratio and the abundance of Sr in the rocks; it was shown (Silant'ev, 2003) that both the carbonation and serpentinization of oceanic peridotites are accompanied by significant Sr enrichment (Fig. 4b). Among the major elements, SiO_2 and MgO are most mobile during the submarine weathering of abyssal peridotites (Snow and Dick, 1995; Bazylev, 1997; Silant'ev et al., 2011). However, even in the most weathered serpentinites, the MgO content does not decrease below 30 wt % and 25 wt % in strongly carbonated varieties (Fig. 3a). Snow and Dick (1995) estimated an MgO loss of up to 5 wt % relative to the initial bulk rock composition during submarine weathering. They also noted a significant

enrichment of abyssal peridotites in K, Na, and Rb during their submarine weathering. Aluminum, Ti, Zr, and Cr are concentrated in secondary phases and accumulate in ultrabasic rocks affected by low-temperature submarine weathering (Snow and Dick, 1995). During the late stage of submarine weathering, serpentinites usually undergo carbonation, while Ca is either adsorbed from seawater or inherited from the protolith (Brady and Gislason, 1997; Silant'ev, 2003). Carbonated serpentinites may contain up to 8–15 wt % CaO and 2900 ppm Sr (Silant'ev, 2003) (Figs. 3b, 4b). The submarine weathering of serpentinites results also in U enrichment (from seawater) and is not accompanied by considerable loss or gain of Fe and Si (Snow and Dick, 1995; Silant'ev, 2003).

It was emphasized above that the enrichment of the altered dunites in quartz makes them sharply different from the known products of peridotite alteration in the oceanic crust. The very high SiO_2 content observed in these rocks is very atypical of MOR peridotites affected by metamorphism and low-temperature weathering (Silant'ev et al., 2009). Relatively high SiO_2 contents were observed only in the MAR serpentinites that underwent peculiar silica metasomatism (Bach and Klein, 2007), which resulted in the steatitization of these rocks and was related to the interaction of serpentinites with the material of gabbroic veins. However, even the most silicified of these serpentinites (known as soapstones) contain no more than 60–66 wt % SiO_2 at 30–32 wt % MgO (Kelemen et al., 2004) (Fig. 3a). According to the calculations of Bach and Klein (2007), the steatitization of serpentinites related to silicic metasomatism occurs at temperatures of $>350^\circ\text{C}$ under the influence of a fluid with high Si activity.

There are only a few studies on mineralogical and geochemical effects related to the subaerial weathering of serpentinites. The weathering of serpentinized peridotites under subaerial conditions is accompanied by the extreme mobilization of MgO, the content of which may decrease in the serpentinites from 40 to 2.5 wt % (Beinlich et al., 2010). During the alteration of primary silicates, silica is initially accommodated in deweylite and, then, accumulates in quartz (opal) (Delvigne et al., 1979; Beinlich et al., 2010). The data of Bulmer and Lavkulich (1994) suggest intense Ni removal during the subaerial weathering of serpentinites. It is relevant to note that the negative correlation of SiO_2 and Ni in the silicified serpentinites of the Stalemate Ridge (Fig. 3f) may indicate that these rocks were produced by the low-temperature alteration of an ultrabasic material, possibly in a subaerial weathering setting.

Beinlich et al. (2010) described the subaerial alteration of clastogenic peridotite fragments from the Devonian conglomerates of the Solund complex (northwestern Norway). The sequential low-temperature alteration of these peridotites resulted in the for-

mation of the following mineral assemblages: (1) serpentine + relicts of primary silicate minerals + magnetite + magnesite \rightarrow (2) deweylite + magnesite + hematite \rightarrow (3) quartz + calcite + hematite. In the case described by Beinlich et al. (2010), the silicification of serpentinites is accompanied by carbonation owing to the input of Ca from the sedimentary country rocks.

Summarizing the available limited data, it can be concluded that the main geochemical effect of the subaerial weathering of ultrabasic rocks is their silicification with the formation of the association of quartz (opal) and iron hydroxides (Delvigne et al., 1979). Perhaps, the volume of aqueous solution and the rate of its percolation through the rock are essential for the character of secondary mineral formation during subaerial weathering. Under humid conditions, primary silicates are dissolved to produce quartz, Fe-montmorillonite (nontronite), and secondary magnetite (Bulmer and Lavkulich, 1994; Andreani et al., 2009). Under arid conditions, the interaction of peridotite with meteoric water results in the extensive precipitation of magnesite and dolomite in carbonate veins, and the formation of carbonates is a relatively rapid process (840–43 000 yr; Kelemen and Matter, 2008).

The data presented above allow us to suppose that the silicification of serpentinites at the Stalemate Fracture Zone occurred at a low temperature and resulted from rock weathering, possibly under subaerial conditions. However, this hypothesis needs to be independently tested, and this was done by means of thermodynamic modeling.

Modeling of the Silicification of Stalemate Fracture Zone Peridotites

The data on the processes of oceanic peridotite alteration reviewed above indicate that the silicification of the Stalemate rocks can be considered as a result of weathering. It is reasonable to consider two settings with contrasting physicochemical parameters for the occurrence of this process, submarine and subaerial. In order to determine which of the two environments was responsible for the silicification of the Stalemate Ridge peridotites, numerical modeling was used in this study.

The method of thermodynamic modeling accounting for the kinetics of mineral dissolution developed by Zolotov and Mironenko (2007) was employed. This approach was implemented in the GEOCHEQ program package (Mironenko et al., 2008). The low-temperature alteration (weathering) of serpentinites was imitated by a great number of aqueous solution waves passing through the same rock volume. Two scenarios with different solution compositions (atmospheric precipitation and seawater) were considered. The duration of a single interaction step was 0.05 yr. Overall, two million waves of aqueous solution passed

through the model serpentine block. The water–rock ratio was estimated from the mass proportion of precipitation and rock affected by weathering for the subaerial scenario and on the basis of rock permeability for the submarine scenario. The water–rock interaction occurred at a temperature of 15°C and a pressure of 1 bar. For the interaction with seawater, hypothetical hydrothermal conditions at temperatures from 50 to 200°C were also modeled. The specific surface area of serpentine was taken to be 1 m²/g (Josef et al., 2007). The specific surface area of quartz (0.02 m²/g; Worley, 1994) was accepted for the calculations of secondary minerals.

In both model scenarios (subaerial and submarine), the kinetic and thermodynamic parameters of the following minerals phases were taken into account: amorphous silica, analcime, aragonite, Ca-montmorillonite, calcite, chrysotile, clinocllore, daphnite, dolomite, Fe-talc, goethite, greenalite, hematite, illite, K-montmorillonite, magnesite, Na-montmorillonite, nontronite (Fe-montmorillonite), siderite, stilbite, and talc. Pyrite and pyrrhotite were also available in the serpentinite–seawater scenario.

The initial composition of serpentine used in the calculations corresponded to sample DR37-14 (Table 2). This rock consists of 70% serpentine, 15% orthopyroxene, 7% clinopyroxene, 5% spinel, and 3% olivine. The choice of this rock rather than a serpentinitized dunite for the initial composition was motivated by the following considerations: (1) the volume proportions of major minerals in the protolith of the silicified dunites cannot be estimated, and (2) the probable differences between the bulk compositions of the protoliths of the serpentinitized lherzolites and dunites cannot affect the character of the main trends of model weathering scenarios. It should also be noted that the above estimate of the chemical characteristics of the altered dunites is rather approximate.

The following compositions of initial minerals were used during modeling: serpentine Mg_{2.5}Fe_{0.5}Si₂H₄O₉, orthopyroxene Mg_{1.69}Ca_{0.05}Na_{0.01}Fe_{0.18}Al_{0.17}Si_{1.91}O₆, clinopyroxene Mg_{0.89}Ca_{0.585}K_{0.07}Na_{0.55}Fe_{0.08}Al_{0.21}Si_{1.91}O₆, spinel Mg_{0.89}Fe_{0.425}Al_{1.79}O₄, and olivine Mg_{1.8}Fe_{0.2}SiO₄. In the submarine scenario, standard seawater with pH = 7.8 interacted with the serpentinite. The composition of rainwater in the subaerial scenario was approximated by pure water with a dissolved CO₂ content corresponding to atmospheric CO₂ pressure (4 × 10⁻⁴ bar) and pH = 5.5. In both cases, the system was open to CO₂.

Modeling of Serpentine Weathering under Ocean Floor Conditions

The modeling of the submarine weathering of serpentinite established the following sequence of primary mineral dissolution: relict orthopyroxene (550 model years) \rightarrow relict olivine (1550 yr) \rightarrow relict cli-

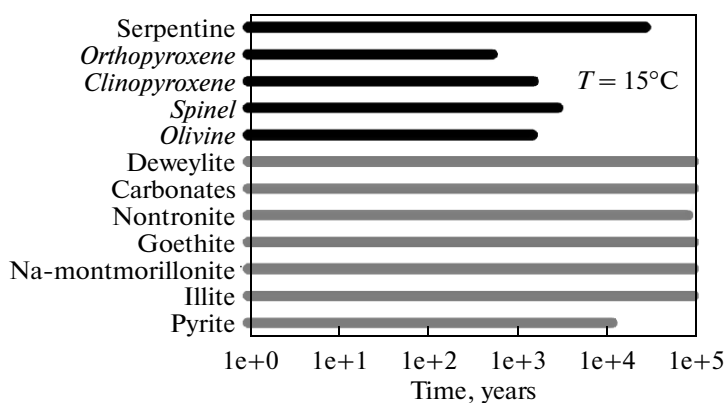


Fig. 5. Evolution of the mineral composition of serpentinite during submarine weathering. Black lines are primary (relative to weathering products) minerals, and gray lines are weathering products.

nopyroxene (1600 yr) → relict spinel (3000 yr) → serpentinite (29 000 yr) (Fig. 5). The secondary mineral association of the initial stage of weathering (≤ 3000 model years) is dominated by talc and deweylite ($\text{Mg}_4\text{Si}_3\text{O}_{10} \cdot 6\text{H}_2\text{O}$, a mixture of crystalline serpentine and talc or serpentine and stevensite). After the dissolution of primary (relative to weathering products) serpentinite, carbonate phases become dominant. At durations of seawater–serpentinite interaction up to 25000 yr, the residue of submarine weathering is enriched in nontronite, but this mineral disappears from the weathering products after the complete dissolution of serpentinite. During the final stage of submarine weathering (100000 model years), the products contain carbonates (dolomite–magnesite, 73 vol %), talc (deweylite) (21 vol %), goethite (3 vol %), Na-montmorillonite (2 vol %), and illite (1 vol %) (Fig. 5). The total volume of the rock increases monotonously during submarine weathering and eventually becomes almost twice that of the initial rock (Table 3).

The bulk composition of serpentinite shows minor changes at the first stage of weathering (≤ 250 model

years) related to the removal of magnesium (by 1.5 wt %) owing to the dissolution of primary silicates and their replacement by talc (deweylite) (Table 3). This process is followed by Mg accumulation accompanying magnesite formation, and its bulk content in the rock increases significantly owing to Mg uptake from seawater. During the whole process of serpentinite–seawater interaction, the mass fraction of Si, Fe, and Al in the rock decreases significantly. However, significant removal or input of these elements was not observed; this is explained by the accumulation of carbonates in the residue, which results in a significant increase in the volume and a proportional decrease in the density of the rock.

A number of model scenarios were also considered for the hypothetical interaction of hot seawater with serpentinite at temperatures of 50, 100, and 200°C. The following variations in the mineral and chemical compositions of the resulting high-temperature residues were observed. At 50°C, the content of carbonates increased, and minor amounts of zeolites were formed in the weathering products. At 100°C, the fraction of zeolites among secondary minerals decreased

Table 3. Tendencies of compositional variations during the submarine weathering of initial serpentinite (sample DR37-14) reconstructed on the basis of thermodynamic modeling

Component	Initial composition	250 yr	2250 yr	14 kyr	100 kyr
SiO ₂	40.66	38.85	29.24	19.92	14.11
Al ₂ O ₃	1.56	2.93	2.07	0.68	0.48
FeO	9.99	9.76	7.58	5.70	4.03
K ₂ O	0.09	0.08	0.05	0.05	0.03
CaO	0.83	3.01	8.40	12.40	14.60
MgO	32.11	29.61	27.47	28.36	29.07
Na ₂ O	0.52	0.15	0.05	0.06	0.04
H ₂ O	14.24	8.53	4.40	2.21	1.57
CO ₂	0	7.10	20.74	30.63	36.07
$V/V_{\text{init}} \times 100\%$	100	111	151	140	198

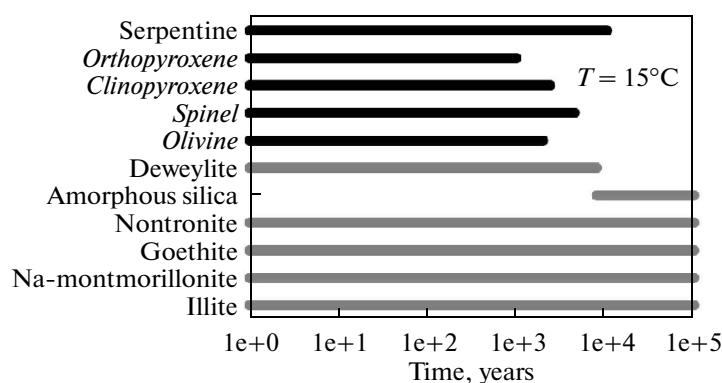


Fig. 6. Evolution of the mineral composition of serpentinite during subaerial weathering. Black lines are primary (relative to weathering products) minerals, and gray lines are weathering products.

significantly, and their formation was not observed at 200°C. The fraction of serpentine in the rock increased with increasing temperature. Clay minerals were not formed in any of the high-temperature scenarios. At 200°C, the final stages of serpentinite interaction with hot seawater produced small amounts of amorphous silica, which, however, could be an artifact of numerical modeling. Changes in the bulk composition of high-temperature residues include a gradual decrease in Mg content and an increase in SiO₂ content with increasing temperature: MgO = 50 wt % (recalculated to the anhydrous composition of the final residue) and SiO₂ = 22.4 wt % at 50°C, MgO = 41.5 wt % and SiO₂ = 48.7 wt % at 100°C, and MgO = 41 wt % and SiO₂ = 51.5 wt % at 200°C.

Thus, the results of model calculations show that the extensive carbonation of serpentinites resulting in a decrease in the relative bulk content of silica can be considered as a mineralogical indicator for submarine weathering. It is evident that the model trends of peridotite compositions at submarine weathering or hydrothermal alteration cannot explain the composition of the silicified serpentinites after dunites from the Stalemate Fracture Zone.

Modeling of Serpentinite Weathering under Subaerial Condition

In this model scenario, the following sequence of primary mineral dissolution was obtained: orthopyroxene (1000 model years) → olivine (2000 yr) → clinopyroxene (2400 yr) → spinel (4500 yr) → serpentine (10 500 yr) (Fig. 6). Despite its low content in the rock, spinel is preserved in the residue longer than any of the primary minerals of the peridotite. Serpentine also shows very low dissolution rates.

The secondary minerals of the initial stage of weathering (<10 000 model years) are dominated by deweylite, which was imitated in models as a serpentine–talc mixture. After the dissolution of the primary serpentinite minerals, deweylite is replaced by amorphous silica. During the final stage of serpentinite weathering (100 000 model years), the newly-formed phases are amorphous silica (72 vol %), goethite (13 vol %), nontronite (12 vol %), illite (2 vol %), and Na-montmorillonite (1 vol %) (Fig. 6). The bulk volume of the rock decreases monotonously during subaerial weathering, reaching 51% of the initial volume after 100 000 model years (Table 4).

Table 4. Tendencies of compositional variations during the subaerial weathering of initial serpentinite (sample DR37-14) reconstructed on the basis of thermodynamic modeling

Component	Initial composition	100 yr	8 kyr	100 kyr
SiO ₂	40.66	42.07	50.00	72.93
Al ₂ O ₃	1.56	2.44	2.70	3.98
FeO	9.99	11.09	11.32	19.18
K ₂ O	0.09	0.09	0.11	0.13
CaO	0.83	0.51	0	0
MgO	32.11	32.83	27.96	0.58
Na ₂ O	0.52	0.27	0.03	0.03
H ₂ O	14.24	10.70	7.89	3.17
$V/V_{\text{init}} \times 100\%$	100	100.08	76.35	51.46

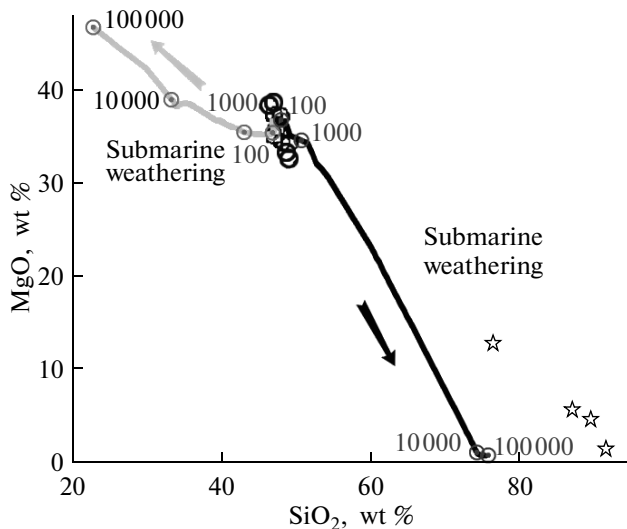


Fig. 7. Main geochemical trends established by the modeling of submarine and subaerial weathering of the serpentinites of the Stalemate Ridge. Numbers indicate the duration of interaction between the rocks and seawater or meteoric water in years. The compositions of rocks were recalculated to a 100% volatile-free basis. Other symbols are the same as in Fig. 3.

Variations in the bulk composition of the serpentinite owing to subaerial weathering are related to significant removal of MgO and CaO (Table 4). The dissolution of Fe–Mg silicates at the subaerial weathering

of serpentinite results in the significant silicification of the initial rock, such that a residue with approximately 73 wt % SiO₂ at 0.58 wt % MgO is formed in the model system (Table 4, Fig. 7).

Based on the results of modeling we arrived at the conclusion that the two types of serpentinite weathering show sharply different geochemical trends and mineralogical characteristics (Fig. 8). The model data indicate also that the geochemical and mineralogical effects observed in the silicified dunites of the Stalemate Ridge are most similar to the expected results of the low-temperature alteration of oceanic serpentinites under subaerial conditions.

GEODYNAMIC INTERPRETATION OF THE WEATHERING CONDITIONS OF THE STALEMATE PERIDOTITES

The empirical and numerical data reported in this paper suggest that the serpentinites of the Stalemate Ridge could hardly be silicified under the conditions corresponding to their present-day deep-sea occurrence and more likely underwent subaerial weathering. The observed evidence of the silicification of serpentinitized lherzolites indicates that these rocks were also weathered under conditions different from those of the ocean floor. The difference in the degree of silicification in the rocks studied (high in the serpentinites after dunites and minor in the serpentinitized lherzolites) can

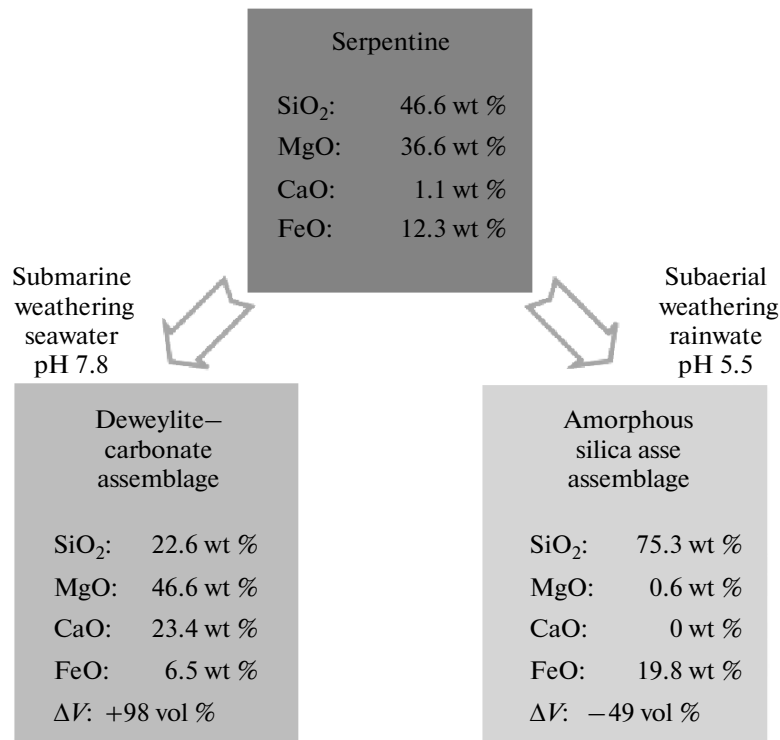


Fig. 8. Variation related to the weathering of serpentinite in submarine and subaerial environments obtained by thermodynamic modeling using the GEOCHEQ program package. The composition of the rock was recalculated to a 100% volatile-free basis.

be attributed to the different positions of these rocks in the section. That is, the serpentinites after dunites were silicified to the highest extent, because they occurred in the uppermost part of the emergent peridotite section most accessible for the infiltration of meteoric waters.

The interpretation of the results of our study inevitably leads to the question about the consistency of the processes that probably took place during the evolution of the ultramafic rocks of the Stalemate Ridge with the tectonics of modern oceanic basins. The answer to this question must evidently be sought in the available evidence on the structure of large transform faults and associating transverse ridges in the Ocean. The best studied examples of such geologic structures are the Vema and Romanche fracture zones in the Atlantic Ocean. These fracture zones are the largest known in the Atlantic and are accompanied by extended transverse ridges, which, similar to the Stalemate Ridge, are divided into blocks and oriented along the direction of the associated fracture zones.

The Vema Fracture Zone shifts the axis of the Mid-Atlantic Ridge by 320 km and associates with an extended transverse ridge, which is approximately 300 km long, up to 30 km wide at the base, and 4 km high. According to Bonatti (1978) and Kastens et al. (1998), this ridge is a slice of the oceanic lithosphere, which was vertically displaced toward the ocean floor. Shallow-water carbonate sediments were found on the summits of two separate blocks of this fragmented ridge. These sediments are 3–4 Ma old and were formed under near-surface (relative to the sea level) conditions (Kastens et al., 1998). The present-day ocean depth in this region is 470–450 m. Bonatti et al. (2005) estimated the rate of uplift for a block of mantle peridotites in the Vema Fracture Zone as 2–4 mm/yr. According to the dating of pelagic carbonate incrustations on peridotites collected at the base of the Vema transverse ridge at various distances from the MAR axis, the ridge was uplifted as a consolidated structure within a tectonically active offset of the Vema Fracture Zone (Bonatti et al., 2005). These authors argued that this uplift resulted in that a significant portion of the transverse ridge (approximately 50 km long) emerged above sea level and was affected by subaerial erosion.

The Romanche transverse ridge (equatorial Atlantic) is located at the northern side of the Romanche Fracture Zone across the eastern intersection of the MAR and the Romanche Fracture Zone (Gasperini et al., 1997). A number of separate blocks of this transverse ridge emerged in the early–middle Miocene above sea level and are now covered with shallow-water carbonate sediments, which were deposited on the subsiding oceanic basement simultaneously with subaerial erosion (Gasperini et al., 1997). The summits of these submersed blocks of the Romanche transverse ridge occur now at a depth of 1000 m. According to the data of seismic profiling and litho-

logical investigations, the ocean floor subsidence of such considerable amplitude began in this region of the crest zone of the Mid-Atlantic Ridge in the early Miocene (Gasperini et al., 1997).

Thus, the available geophysical and geological data indicate that one characteristic feature of the tectonic evolution of transverse ridges associating with large transform zones in the Ocean is their vertical movements of varying amplitude and direction. This suggests that the subaerial weathering of peridotites in the Stalemate transverse ridge could be related to such vertical movements. It is also possible that vertical movements at the Stalemate Fracture Zone were triggered by the tectonic upthrust of an oceanic lithospheric block of Cretaceous (?) age along the Kula–Pacific Fracture Zone (Lonsdale, 1988). The reasons for this tectonic event should probably be sought in the location of the ocean region considered between two important geologic structures, which influenced the tectonic evolution of the northwestern Pacific: the Emperor Ridge in the southwest and the frontal part of the Aleutian subduction zone in the north and northwest.

The interpretation proposed in this paper for the formation conditions of silicified peridotites in the Stalemate Ridge cannot evidently be claimed as final. Since the methods of isotopic geochemistry may provide important information on the nature of the main agents and physicochemical parameters of peridotite alteration, a very important test for the plausibility of the silicification model proposed in this paper can be provided by the investigation of O and Sr isotopic compositions in these rocks, which is planned by the authors for the near future. The conclusions drawn on the basis of the presented data give rise to several question that cannot yet be answered: (1) where and when did the subaerial weathering of the peridotite of the Stalemate Fracture Zone occur, and (2) what was the tectonic event that caused the subsidence of an oceanic lithospheric block to a depth of 4000 m, and how long did it take?

CONCLUSIONS

The comprehensive petrological and geochemical investigation of altered (including silicified) peridotites dredged during cruise SO201-1b of the joint Russian–German expedition on the R/V *Sonne* on the eastern slope of the northwestern segment of the Stalemate transverse ridge revealed remarkable enrichment of serpentinites after dunites in amorphous silica and quartz and unusually high SiO₂ (up to 88.7 wt %) and low MgO contents (up to 1.4 wt %) in them. These mineralogical and geochemical features clearly distinguish these rocks from the known products of the hydrothermal alteration and low-temperature weathering of peridotites in the oceanic crust. The results of numerical modeling and the analysis of published data allowed us to suppose that the geochemical and mineralogical effects observed in the silicified dunites of

the Stalemate Fracture Zone are consequences of the low-temperature deserpentinization of oceanic rocks under subaerial conditions. Hence, the peridotites could not be weathered under the conditions corresponding to their present-day submarine occurrence at depths of approximately 4000 m. This implies that the oceanic crustal block of the northwestern Pacific discussed in this paper has experienced, since the time of its formation, uplift followed by subsidence with amplitudes of several thousand meters.

ACKNOWLEDGMENTS

We are grateful to Captain L. Mallon and the crew of the R/V *Sonne* for the fruitful cooperation during the cruise, which was a prerequisite for the success of the expedition. Thanks are also due to M.V. Mironenko (Vernadsky Institute of Geochemistry and Analytical Chemistry, Russian Academy of Sciences) for providing the program and the database and B.A. Bazylev (Vernadsky Institute of Geochemistry and Analytical Chemistry, Russian Academy of Sciences) for valuable comments on the mineralogy of the medium-temperature metamorphism of oceanic mantle peridotites.

This study was financially supported by the German–Russian project KALMAR, the Russian Foundation for Basic Research (project no. 09-05-00008), and Program P-21 of the Presidium of the Russian Academy of Sciences “Fundamental Problems of Oceanology: Physics, Geology, Biology, and Ecology” (Theme “Interaction of Magmatic and Hydrothermal Systems in the Oceanic Lithosphere and Mineral Resources”).

REFERENCES

- Andreani, M., Luquot, L., Gouze, P., Godard, M., Hoise, E., and Gibert, B., Experimental Study of Carbon Sequestration Reactions Controlled by the Percolation of CO₂-Rich Brine Through Peridotites, *Environ. Sci. Technol.*, 2009, vol. 43, pp. 1226–1231.
- Bach, W. and Klein, F., Silica Metasomatism of Oceanic Serpentinites, *Goldschmidt Conference*, 2007, A48.
- Bazylev, B.A., Allochemical Metamorphism of Mantle Peridotites in the Hayes Fracture Zone of the North Atlantic, *Petrology*, 1997, vol. 5, no. 4, pp. 322–337.
- Beinlich, A., Austrheim, H., Glodny, J., Erambert, M., and Andersen, T.B., CO₂ Sequestration and Extreme Mg Depletion in Serpentinized Peridotite Clasts from the Devonian Solund Basin, SW-Norway, *Geochim. Cosmochim. Acta*, 2010, vol. 74, pp. 6935–6964.
- Bonatti, E., Brunelli, D., Buck, W.R., Cipriani, A., Fabbretti, P., Ferrante, V., Gasperini, L., and Ligi, M., Flexural Uplift of a Lithospheric Slab Near the Vema Transform (Central Atlantic): Timing and Mechanisms, *Earth Planet. Sci. Lett.*, 2005, vol. 240, nos. 3–4, pp. 642–655.
- Bonatti, E., Vertical Tectonism in Oceanic Fracture Zones, *Earth Planet. Sci. Lett.*, 1978, vol. 37, no. 3, pp. 369–379.
- Brady, P.V. and Gislason, S.R., Seafloor Weathering Controls on Atmospheric CO₂ and Global Climate, *Geochim. Cosmochim. Acta*, 1997, vol. 61, no. 5, pp. 965–973.
- Bulmer, C.E. and Lavkulich, L.M., Pedogenic and Geochemical Processes of Ultramafic Soils Along a Climatic Gradient in Southwestern British Columbia, *Canadian J. Soil Sci.*, 1994, vol. 74, pp. 165–177.
- Delvigne, J., Bisdom, E.B.A., Sleeman, J., and Stoops, G., Olivines, Their Pseudomorphs and Secondary Products, *Pedologie*, 1979, vol. 29, pp. 247–309.
- Erickson, B.H. and Grim, P.J., Profiles of Magnetic Anomalies South of Aleutian Island Arc, *Geol. Soc. Am. Bull.*, 1969, vol. 80, pp. 1387–1390.
- FS Sonne. Fahrbericht. Cruise Report SO201-1b. Kalmar, no. 2009. http://www.ifm.-geomar.de/fileadmin/ifm-geomar/fuer_alle/institut/publikationen/ifm-geomar_rep32.pdf. pp. O201–1.
- Fullam, T.J., Supko, P.R., and Boyce, R.E., Some Aspects of Late Cenozoic Sedimentation in the Bering Sea and North Pacific Ocean, *DSDP Init. Rept.*, 1973, vol. 19, pp. 887–896.
- Gasperini, L., Bonatti, E., Ligi, M., Sartori, R., Borsetti, A., Negri, A., Ferrari, A., and Sokolov, S., Stratigraphic Numerical Modeling of a Carbonate Platform on the Romanche Transverse Ridge, Equatorial Atlantic, *Mar. Geol.*, 1997, vol. 136, pp. 245–257.
- Grim, P.J. and Erickson, B.H., Fracture Zones and Magnetic Anomalies South of Aleutian Trench, *J. Geophys. Res.*, 1969, vol. 74, pp. 1488–1494.
- Jochum, K.P., Wang, X., Mertz-Kraus, R., Nohl, U., Schmidt, S., Schwager, B., Stoll, B., Qichao, Yang Q., and Weis, U., Geostandards and Geoanalytical Research, *Bibliographic Rev.*, 2009, vol. 34, no. 4, pp. 407–410.
- Josef, J.A., Fisk, M.R., and Giovannoni, S., Peridotite Dissolution Rates in Microbial Enrichment Cultures, *Proc. Ocean Drilling Program, Sci. Res.*, Kelemen, P.B., Kikawa, E., and Miller, D.J., Eds., 2007, vol. 209, pp. 1–38.
- Kastens, K., Bonatti, E., Caress, D., Carrara, G., Dauteuil, O., Frueh-Green, G., Ligi, M., and Tartarotti, P., The Vema Transverse Ridge (Central Atlantic), *Mar. Geophys. Res.*, 1998, vol. 20, pp. 533–556.
- Kelemen, P.B. and Matter, J., In Situ Carbonation of Peridotite for CO₂ Storage, *Proc. Natl. Acad. Sci. USA*, 2008, vol. 105, no. 45, pp. 17295–17300.
- Kelemen, P.B., Kikawa, E., Miller, D.J., et al., Alteration of Abyssal Peridotite-Initial Results of Ocean Drilling Program Leg 209 (Mid-Atlantic Ridge, 15°N), *EGU meeting, Proc. Ocean Drilling Program, Init. Rept.*, 2004, vol. 209, pp. 25–30. doi:10.10.2973/odp.proc.ir.209.2004.
- Krasnova, E., Portnyagin, M., Silantiev, S., Werner, R., Hauff, F., and Hoernle, K., Major and Trace-Element Geochemistry of Ultramafic Rocks from the Stalemate Fracture Zone (NW Pacific), *Goldschmidt Conference*. 2011.
- Lonsdale, P., Paleogene History of the Kula Plate: Offshore Evidence and Onshore Implications, *Geol. Soc. Am. Bull.*, 1988, vol. 100, pp. 733–754.
- Mironenko, M.V., Melikhova, T.Yu., Zolotov, M.Yu., and Akinfiyev, N.N., GEOSHEQ_M—A Complex for Thermodynamic and Kinetic Modeling of Geochemical Systems. Ver. 2008, Vestn. OGGGN RAN, 2008, no. 1/ URL:http://www.scgis.ru/russian/cp1251/h_dgggms/1-2008/informbul-1_2008/mineral-22.pdf.

- Rea, D.K. and Dixon, J.M., Late Cretaceous and Paleogene Tectonic Evolution of the North Pacific Ocean, *Earth Planet. Sci. Lett.*, 1983, vol. 64, pp. 67–73.
- Ryan, W.B.F., Carbotte S.M., Coplan J.O., O'Hara S., Melkonian A., Arko R., Weissel R.A., Ferrini V., Goodwillie A., Nitsche F., Bonczkowski J., Zemsky R., Global Multi-Resolution Topography Synthesis, *Geochem. Geophys. Geosyst.*, 2009, vol. 10, no. Q03014, p. 9.
- Shipboard Scientific Party, Introduction to Leg 145: North Pacific Transect, *Proc. Ocean Drilling Program, Init. Rept.*, 1993, vol. 145, pp. 5–7.
- Silantyev, S.A., Krasnova, E.A., Kannat, M., Bortnikov, N.S., Kononkova, N.N., and Bel'tenev, V.E., Peridotite–Gabbro–Trondhjemite Association of the Mid-Atlantic Ridge between 12°58' and 14°45'N: Ashadze and Logachev Hydrothermal Vent Fields, *Geochem. Int.*, 2011, no. 4, pp. 323–354.
- Silantyev, S.A., Mironenko, M.V., and Novoselov, A.A., Hydrothermal Systems in Peridotites of Slow-Spreading Mid-Oceanic Ridges. Modeling Phase Transitions and Material Balance: Downwelling Limb of a Hydrothermal Circulation Cell, *Petrology*, 2009, vol. 17, no. 2, pp. 138–157.
- Silantyev, S.A., Variations in the Geochemical and Isotopic Characteristics of Residual Peridotites along the Mid-Atlantic Ridge as a Function of the Nature of the Mantle Magmatic Sources, *Petrology*, 2003, vol. 11, no. 4, pp. 305–326].
- Snow, J.E. and Dick, H.J.B., Pervasive Magnesium Loss by Marine Weathering of Peridotite, *Geochim. Cosmochim. Acta*, 1995, vol. 59, pp. 4219–4235.
- Wessel, P. and Smith, W.H.F., The Generic Mapping Tools (GMT), Version 3.0, *Technical Reference Cookbook*, SOEST/NOAA, 1995.
- Worley, W.R., *Dissolution Kinetics and Mechanisms in Quartz- and Granite-Water Systems, Massachusetts: Massachusetts Inst. Technol.*, 1994.
- Zolotov, M.Yu. and Mironenko, M.V., Timing of Acid Weathering on Mars: A Kinetic-Thermodynamic Assessment, *J. Geophys. Res.*, 2007, vol. 112, p. E07006.